JOC The Journal of Organic Chemistry

Article

pubs.acs.org/joc

Platinum(II)-Catalyzed Cyclization Sequence of Aryl Alkynes via C(sp^3)−H Activation: A DFT Study

Zhi-Feng Li,[†,‡] Yanzhong Fan,[†] Nathan J. DeYonker,[§] Xiting Zhang,[†] Cheng-Yong Su,[†] Huiying Xu,[†] Xianyan Xu,[†] and Cunyuan Zhao*[,†]

[†]MOE Key Laboratory of Bioinorganic and Synthetic Chemistry/KLGHEI of Environment and Energy Chemistry, School of Chemistry and Chemical Engineering, Sun Yat-Sen University, Guangzhou 510275, People's Republic of China

[‡]College of Life Science and Chemistry, Tianshui Normal University, Tianshui 741001, China

[§]Department of Chemistry, The University of Memphis, Memphis, Tennessee 38152-3550, United States

Supporting Information

ABSTRACT: The mechanism and intermediates of hydroalkylation of aryl alkynes via C(sp^3)−H activation through a platinum(II)-centered catalyst are investigated with density functional theory at the B3LYP/[6-31G(d) for H, O, C; 6-31+G(d,p) for F, Cl; SDD for Pt] level of theory. Solvent effects on reactions were explored using calculations that included a polarizable continuum model for the solvent (THF). Free energy diagrams for three suggested mechanisms were computed: (a) one that leads to formation of a Pt(II) vinyl carbenoid (Mechanism A), (b) another where the transition state implies a directed 1,4-hydrogen shift (Mechanism B), and (c) one with a Pt-aided 1,4-hydrogen migration (Mechanism C). Results suggest that the insertion reaction pathway of Mechanism A is reasonable. Through 4,5-hydrogen transfer, the Pt(II) vinyl carbenoid is formed. Thus, the stepwise insertion mechanism is favored while the electrocyclization mechanism is implausible. Electron-withdrawing/electron-donating groups substituted at the phenyl and benzyl sp^3 C atoms slightly change the thermodynamic properties of the first half of Mechanism A, but electronic effects cause a substantial shift in relative energies for the second half of Mechanism A. The rate-limiting step can be varied between the 4,5-hydrogen shift process and the 1,5-hydrogen shift step by altering electron-withdrawing/electron-donating groups on the benzyl C atom. Additionally, NBO and AIM analyses are applied to further investigate electronic structure changes during the mechanism.

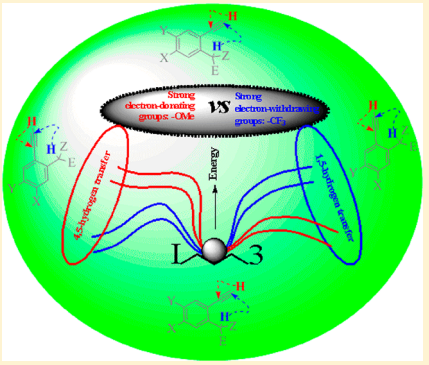

1. INTRODUCTION

Although transition-metal (TM)-catalyzed C(sp^3)−H bond functionalization is valuable in synthetic organic chemistry,[1] activation of C(sp^3)−H bonds is still considered a difficult challenge because of their high dissociation energy.[2] To date, transition-metal catalysts have emerged as an alternative to conventional C−C bond-forming reactions through cleavage of activated or inactive C(sp^3)−H bonds. Despite significant progress in this area, such as rhodium-centered reactions,[3] catalytic transformations of C(sp^3)−H bonds to C−C bonds with platinum catalysts still remain rare.[4]

Shilov and co-workers' study[5] of the platinum(II)-catalyzed oxidation of methane to methanol in 1972 initiated extensive investigation of C(sp^3)−H bond activation with platinum-centered complexes.[4a−d,6] Nowadays, catalysis with electrophilic metal salts is a rapidly evolving area of research for development of new reactions triggered by π-activation of alkynes. Recently, Pt-centered catalysts have shown their efficiency in a series of transformations involving the transfer of a nucleophilic group onto an alkyne, followed by ring closure on the resulting carbocationic intermediate.[7] For example, Pt-catalyzed intermolecular hydroalkylation of aryl alkynes provides a convenient access to highly functionalized indenes,[4a−d] which are abundant in natural products and pharmaceuticals.[8] The hydroalkylation of terminal alkynes has been reported to give substituted indenes via an overall cyclization (Scheme 1).[4a−c,9] These formal cycloisomerizations were proposed to proceed via the initial formation of a Pt−vinylidene species, and three mechanistic pathways were proposed: (1) direct or concerted insertion of the Pt−vinylidene into the benzylic C−H bond,[4a] (2) a 1,5-sigmatropic hydrogen shift along the π system,[4b,c] and (3) a sequence of a hydride transfer from the benzylic position to this latter species, followed by ring closure.[4c] The above three pathways were hypothesized based on a 1,5-hydrogen transfer step. However, the reasons that 1,5-hydrogen shifting is favored over 1,4-hydrogen shifting in the reaction of Pt-catalyzed intramolecular cyclization of aryl alkynes are unclear.

The remarkable progress in the hydroalkylation of terminal alkynes has mostly been focused on synthesis and characterization of new complexes, without utilizing computational chemistry to validate mechanistic speculation.[4c] Although a few

Received: May 2, 2012
Published: July 2, 2012

   dx.doi.org/10.1021/jo300849t | J. Org. Chem. 2012, 77, 6076−6086

Scheme 1. Hydrogen Transfer onto a Metal−Vinylidene/Cyclization Sequence

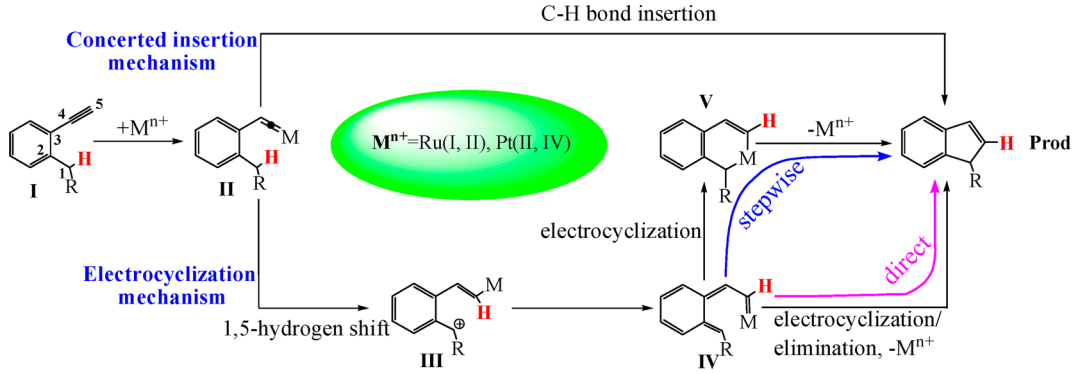

Scheme 2. Three Plausible Mechanisms Were Envisioned for This Novel Pt-Catalyzed Transformation

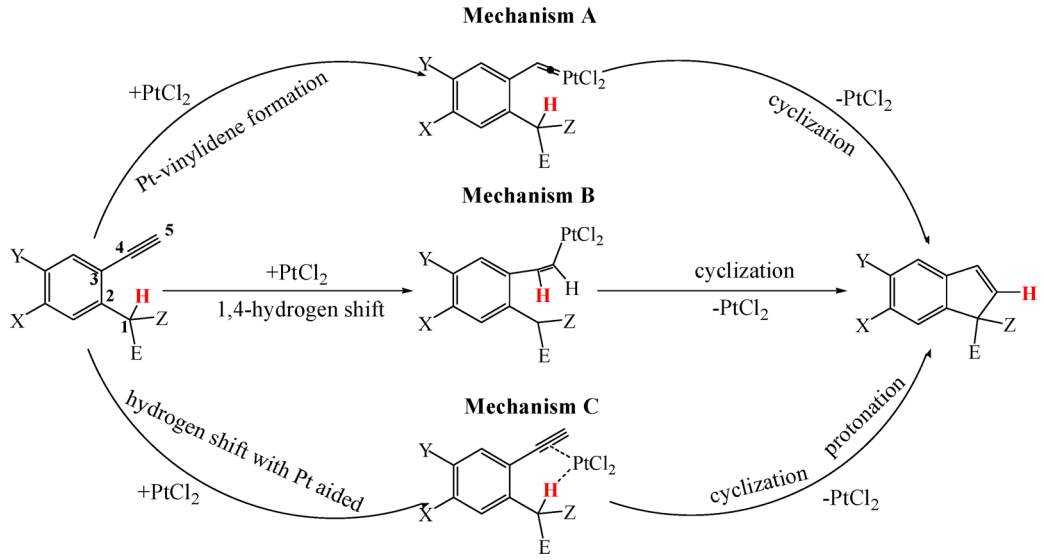

groups have discussed the mechanism of this type of reaction,[4a−d] there are few detailed theoretical studies available in the literature where mechanistic possibilities are compared for the Pt(II)-catalyzed transformation.[4a−d] Hence, in this paper, we present a thorough density functional theory (DFT) computational investigation of the mechanism of the Pt(II)-catalyzed synthesis of highly substituted indenes.[4a−d]

We attempt to gain detailed insight on the catalytic mechanism by employing DFT calculations to examine the following aspects of the reaction: how the substrate and the catalyst bind to a complex; how the different substrate substituents influence the reaction; the identity of the rate-limiting step of the whole transformation;[10] whether or not other reaction modes exist, such as Pt-aided catalysis;[4d,11] whether or not the insertion mechanism is a direct or concerted process; and, finally, to qualitatively examine the origin of electronic interactions. Three plausible mechanisms (Mechanisms A, B, and C in Scheme 2) were proposed in which X = H, Y = H, E = Me, and Z = OMe. This will be referred to as the model substrate (MODs).[12]

It is important to note, however, in this type of catalytic process[4a−d] that there is no direct physical evidence for the putative intermediates, and therefore, the experimental mechanisms are largely proposed on the basis of reaction outcomes. Therefore, a better understanding of the nature of the reactive species is highly desirable, as it would strongly increase the predictive power and lead to improved rational catalyst design.

2. COMPUTATIONAL METHODS

The geometries of all the structures were fully optimized by hybrid density functional theory (DFT)[13] using the Gaussian 09 program suite.[14] The hybrid B3LYP[15] and BHandHLYP[15b,16] density functionals were used in conjunction with the standard 6-31G(d)/6-31G(d,p) basis set for the nonmetal atoms[17] (6-31+G(d,p) for Cl and F) and the SDD pseudo potential for the Pt center.[7b] This computational method has been successfully applied in the mechanistic studies of transition-metal catalysis.[18] Unscaled harmonic vibrational frequency calculations were used to characterize all of the stationary points as either minima or transition states. Intrinsic reaction coordinates (IRC)[19] were employed to verify the connection of the transition states to two relevant minima. To include the effect of the solvent on the reactions of interest, the polarized continuum model (PCM)[20] with UFF sets of radii was applied and single-point energy calculations were done at the B3LYP/PCM/6-31+G(d,p) [SDD for Pt]//B3LYP/6-31G(d) [6-31+G(d,p) for Cl, F; SDD for Pt] level of theory using the geometries along the minimum energy pathway. The dielectric constant was assumed to be 7.58 for the bulk solvent THF. The natural bond orbital (NBO) analysis was also carried out using the NBO 5.0 procedure.[21] Atoms-in-molecules (AIM) analyses were performed with the AIMALL program.[22]

To test the reliability of the different functions and basis sets, we have also calculated and compared the reaction barriers for the insertion reaction pathways of Mechanism A using B3LYP/6-31G(d,p) [(6-31+G(d,p) for Cl; SDD for Pt] and BHandHLYP/6-31G(d) [6-31+G(d,p) for Cl; SDD for Pt] methods. The calculated reaction barriers are qualitatively similar to each other (within a few kcal/mol) and close to relative energies obtained at the B3LYP/6-31G(d) [6-31+G(d,p) for Cl; SDD for Pt] level of theory (see Figure 1 and Table

dx.doi.org/10.1021/jo300849t | J. Org. Chem. 2012, 77, 6076−6086

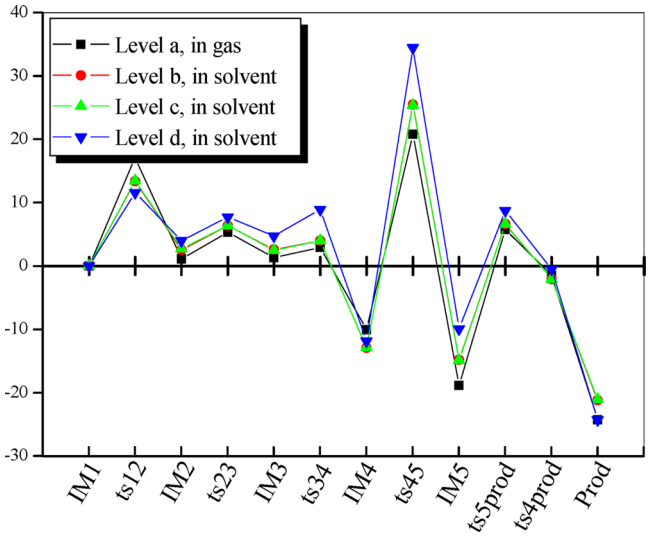

Figure 1. Comparison of the relative free energies (kcal/mol) for the complexes and the transition states for the pathways of Mechanism A at four calculated levels: a, b, c, and d.[23]

1). It shows that the B3LYP/6-31G(d) [6-31+G(d,p) for Cl and F; SDD for Pt] is adequate to determine the geometries and the thermodynamics parameters of this type of catalytic reaction. Therefore, throughout the paper, we discuss only the results from the B3LYP/6-31G(d) [6-31+G(d,p) for Cl and F; SDD for Pt] level of theory.

3. RESULTS AND DISCUSSION

The optimized geometries for the reactants, intermediates (**IM**), transition states (**ts**), and product complex (**Prod**) of the reactions are depicted schematically in Figure 2. From the literature,[4a−d,7b,11,24] we examined the detailed reaction mechanisms for Pt-catalyzed C(sp^3)−H activation/C−C bond formation reactions depicted in Scheme 2. A methoxy complex of *o*-substituted aryl alkynes was chosen as a model system, which is representative of experiments.[4c,7b] In the paper, the transition state between intermediates **IM*m*** and **IM*n*** is denoted as **ts*mn***, while **ts*m*Prod** denotes the transition state between the intermediate **IM*m*** and **Prod**.

3.1. Mechanism A: Pt−Vinylidene Formation. It is a generally accepted that the Pt-catalyzed cyclization begins from the coordination of Pt to the nucleophilic center (or centers) of the substrate.

However, experimental evidence supporting the structure of the reactive intermediates is still lacking.[4b−d,11] We, therefore, looked for the possible structures of such complexes. Figure 2 shows the optimized structures of two intermediates (**IM1** and **IM1′**) corresponding to the initial coordination stage. It is observed that the Pt(II) in **IM1** is attacked by the nucleophilic center alkyne group, and in **IM1′**, both the methoxy and the alkyne groups interact with Pt(II). To investigate if either **IM1** or **IM1′** can be associated with this energy profile, we have computed the relative energies of the first reaction step. It is seen in Figure 3 that **ts1′2′** has a higher energy barrier of 45.3 kcal/mol, compared with 13.4 kcal/mol of **ts12** relative to **IM1**. On the other hand, **IM1′** has a higher energy (8.9 kcal/mol) relative to **IM1**. Therefore, the pathway beginning from **IM1** will be discussed in detail below.

First, we investigated the electronic structure of **IM1** using the Dewar−Chatt−Duncanson (DCD) model[25] and NBO, AIM,[26] and NRT (natural resonance theory) analyses. The results indicate that the main interactions in **IM1** are donation TM $\overset{\sigma}{\leftarrow}$ L and its back-donation interaction TM $\overset{\pi_{\parallel}}{\rightarrow}$ L. The interaction is electrostatic in nature. The σ_{C5-H2} MO interacts with σ^*_{C4-C5} and σ^*_{C3-C4} in **IM1**, which should not only spur the 4,5-hydrogen shift but also elongate the C4−C5 and C3−C4 bonds. For a detailed discussion of the **IM1**, see the Supporting Information (pages S27 and S28).

Table 1. Thermodynamic Properties (Relative Free Energy and Activation Free Energy in Solution, kcal/mol) of the Structures in Mechanism A

system		complex	ts12	IM2	ts23	IM3	ts34	IM4	ts45	IM5	ts5Prod	ts4Prod	Prod
MODs	ΔG^{rel}_{gas}	0.0	17.1	1.1	5.3	1.3	2.9	−10.1	20.8	−18.9	5.7	−1.5	−24.3
	$\Delta G^{\ddagger}_{gas}$		17.1		4.2		1.6		30.9		24.6	8.6	
	ΔG^{rel}_{sol}	0.0	13.4	2.6	6.3	2.6	4.0	−13.0	25.5	−14.9	6.6	−2.1	−21.2
	$\Delta G^{\ddagger}_{sol}$		13.4		3.8		1.4		38.4		21.5	10.9	
	$\Delta G^{rel}_{sol}{}^{a}$	0.0	13.4	2.7	6.4	2.5	4.0	−12.9	25.3	−14.9	6.6	−2.1	−21.1
	$\Delta G^{\ddagger}_{sol}{}^{a}$		13.4		3.7		1.5		38.2		21.5	10.8	
	$\Delta G^{rel}_{sol}{}^{b}$	0.0	11.6	4.0	7.7	4.7	8.9	−11.9	34.5	−9.9	8.7	−0.5	−24.3
	$\Delta G^{\ddagger}_{sol}{}^{b}$		11.6		3.7		4.1		46.4		18.7	11.4	
S1	ΔG^{rel}_{sol}	0.0	14.5	1.6	5.9	2.2	4.1	−12.3	24.2	−15.9	8.0	0.1	−21.5
	$\Delta G^{\ddagger}_{sol}$		14.5		4.3		1.9		36.5		23.9	12.4	
S2	ΔG^{rel}_{sol}	0.0	14.1	2.1	5.5	1.5	3.0	−11.7	25.2	−16.5	7.4	−0.4	−21.9
	$\Delta G^{\ddagger}_{sol}$		14.1		3.5		1.6		36.8		23.9	11.3	
S3	ΔG^{rel}_{sol}	0.0	16.0	6.1	10.6	6.8	8.7	−7.6	32.4	−10.6	9.7	0.4	−18.0
	$\Delta G^{\ddagger}_{sol}$		16.0		4.5		1.9		40.1		20.3	8.0	
S4	ΔG^{rel}_{sol}	0.0	13.4	2.2	6.5	3.1	3.4	−15.8	24.3	−16.1	5.9	−2.2	−21.5
	$\Delta G^{\ddagger}_{sol}$		13.4		4.3		0.2		40.1		22.1	13.6	
S5	ΔG^{rel}_{sol}	0.0	14.4	2.7	6.4	3.5	21.3	9.9	34.8	−0.9	24.9	14.3	−21.9
	$\Delta G^{\ddagger}_{sol}$		14.4		3.7		17.8		24.9		25.8	4.4	
S6	ΔG^{rel}_{sol}	0.0	14.1	1.8	8.4	3.5	5.0	−20.0	20.6	−20.7	8.2	0.3	−19.7
	$\Delta G^{\ddagger}_{sol}$		14.1		6.6		1.6		40.5		28.9	20.3	

[a]Obtained with the B3LYP method at 6-31G(d,p) for C, H, O, F, Cl; SDD for Pt. [b]Obtained with the BHandHLYP method at 6-31G(d) for C, H, and O; 6-31+G(d,p) for F and Cl; SDD for Pt.

dx.doi.org/10.1021/jo300849t | J. Org. Chem. 2012, 77, 6076−6086

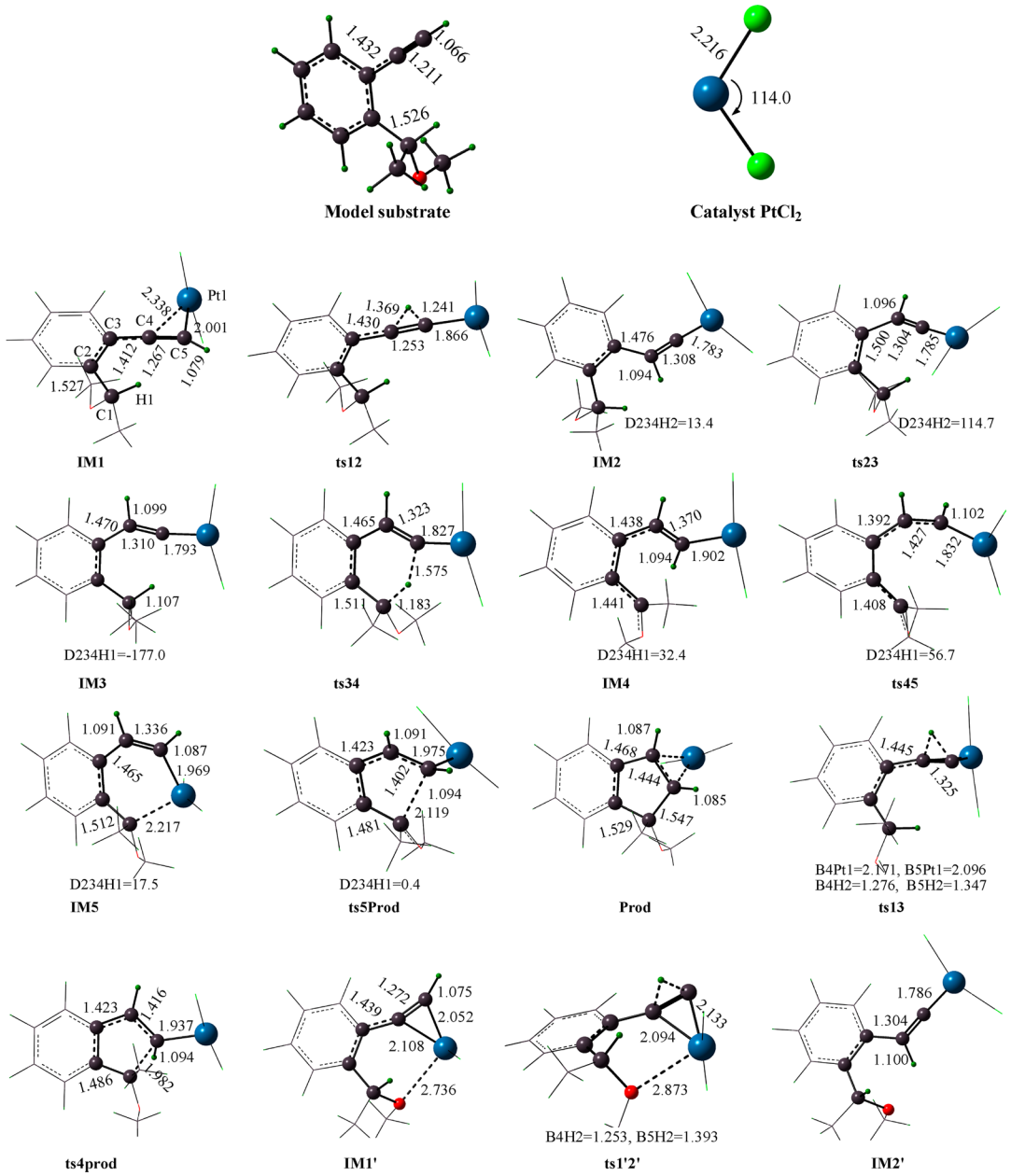

Figure 2. Schematic diagrams of the optimized geometries for Mechanism A reactions and partial geometries for Mechanisms B and C between the model substrate and the $PtCl_2$ catalyst (bond length, Å; angle, deg).

As mentioned above, Mechanism A could be completed through a direct hydrogen transfer from C5 to C4[4a−d,11,24] and subsequent formation of the Pt−vinylidene complexes. The indenes could then be formed either by a direct insertion of the metal−vinylidene into the benzylic C−H or by a sequence of hydride transfers from the benzylic position to this latter species, followed by ring closure, or by a hydrogen shift/electrocyclization sequence. In **ts12**, the C3−C4 bond length is elongated by 0.018 Å (from 1.412 to 1.430 Å), and the electron occupancy of $\sigma^*_{C4-C5}/\sigma^*_{C3-C4}$ increases from 0.020/0.032 e (in **IM1**) to 0.128/0.034 e (in **ts12**). However, the bond length of C4−C5 is 1.253 Å in **ts12**, slightly shorter than that in **IM1** (1.267 Å), which contradicts the above forecast that this bond length will be increased by σ^* antibonding. In **ts12**, the NPA (natural population analysis) charges indicate that electrostatic interaction between C4 (−0.030 e) and C5 (−0.146 e) with H2 (0.408 e) leads to the formation of a three-membered ring that possesses a tightened C4−C5 bond and competes with the antibonding character of the C4−C5 MO. A new and stable structure, **IM2**, is formed from **ts12**. Figure 3 shows that the free energy of activation was calculated to be 13.4 kcal/mol for **ts12** and the free energy of reaction was 2.6 kcal/mol for the **IM2** with respect to **IM1**. **IM2** is a Pt−vinylidene because the C5−Pt bond is shortened to 1.783 Å (the extent is about 10%). **IM2** leads to **ts23**, with a dihedral angle D234H2 changing from 13.4° to −177.0°, and the Pt−vinylidene **IM3** is generated.[27] This Pt−vinylidene intermediate, a **TM** carbene complex, is proposed in several papers.[4a−d,7b,24]

It is interesting that **IM2** and **IM3** have significantly different geometries,[28] while their energetic difference is very small (only about 1 kcal/mol). To investigate this phenomenon, we performed an energetic analysis with NBO deletions. This

dx.doi.org/10.1021/jo300849t | J. Org. Chem. 2012, 77, 6076−6086

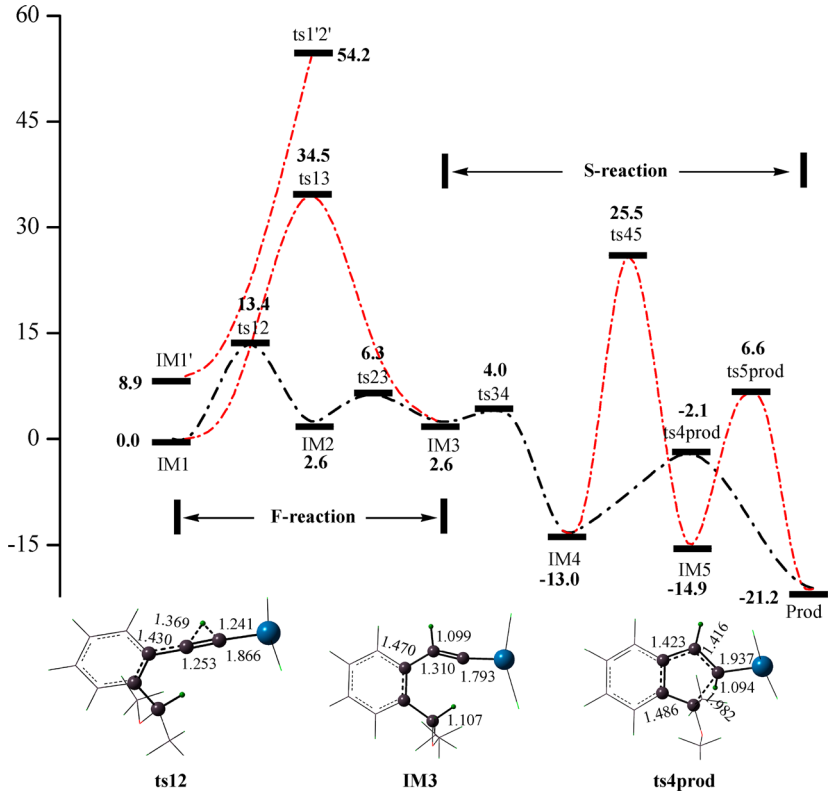

Figure 3. Energy profiles (kcal/mol) for Mechanism A. The relative free energies are given considering solvation effects [values were calculated at the B3LYP/PCM/6-31+G(d,p) (SDD for Pt)//B3LYP/6-31G(d) (6-31+G(d,p) for Cl; SDD for Pt) level using single-point PCM calculations to model the effect of the solvent (THF)].

shows that the localized contribution favors **IM2** and the delocalization contribution favors **IM3** by a similar amount (about 17 kcal/mol), leading to nearly equal total energies for the two isomers.[29] In this process, the interaction between σ_{C4-H2} and n^*_{C5} is strengthened in **IM3** by over about 10 kcal/mol, contrasting to that in **IM2**.

According to a series of criteria,[30] the **TM** carbenes are divided into two classes, which are Fischer carbenes[31] and Schrock carbenes.[32] The carbene carbon atom C5 of **IM3** is electrophilic (NPA charge is 0.174 e) and possesses a stabilizing π-donor alkynyl group. Pt is a late transition metal, and further based on the nature of the Pt−C5 bond,[33] the Pt−vinylidene **IM3** can be unambiguously classified as a Fischer-type carbene rather than a Schrock-type carbene.[30−32,34] The conjugated complex **IM3** can be formed via π-activation of an alkyne moiety under the influence of alkynophilic metal salts. Interestingly, although the energy of vinylidene complex **IM3** is comparable to that of the vinylidene complex **IM2**, the C1−H1 bond length and the distance between H1 and C5 are shorter in **IM3**, which favors the $\sigma_{C1-H1} \rightarrow n^*_{C5}$ interaction, with 3.5 kcal/mol of secondary stabilization energy $E^{(2)}_{ij}$. Also, as a Fischer-type carbene, the NPA charge of the **IM3** $C5_{2p\pi}$ orbital indicates electron deficiency (0.688 e, just above half an electron) in the region exposed to electrophilic attack.[30b,31] In contrast, the NPA charge of the $H1_{1s}$ orbital in **IM3** is 0.782 e, together with the electron-deficient $C5_{2p\pi}$ orbital undergoing a donor−acceptor mechanism; this exemplifies Fischer-type carbene character.[30b,34] Thus, the further 1,5-hydrogen transfer process is feasible.[4c] In **ts34**, a hydride-transfer process occurs, which has also been identified in the rhodium-centered catalysis.[3,35] It is the first time that the free energy of **IM4** is much lower (about 13.0 kcal/mol) than that of the precursor Pt−π complex **IM1**. **IM4** has two competing pathways due to differing mechanisms for the ring closure.[4a−d,24,36] It can be seen from Figure 3 that **IM4** can be derived either by an electrocyclization/elimination sequence, **IM4** → **ts45** → **IM5** → **ts5Prod** → **Prod**, or via an insertion step, **IM4** → **ts4Prod** → **Prod**. In the electrocyclization/elimination sequence, both **ts45** and **ts5Prod** have a high free energy of activation, 38.5 and 21.5 kcal/mol, respectively. Therefore, the insertion pathway of **IM4** → **ts4Prod** → **Prod** is favored. As shown in Figure 3, the **ts4Prod** only has a 10.9 kcal/mol activation free energy, which is overall lower than that of **IM1**, and therefore, the follow-up insertion step **IM4** → **ts4Prod** → **Prod** is a facile process in this catalysis.

It is necessary to mention that the indenes can be derived in two ways. The first is from aryl alkynes via C(sp^3)−H activation by the benzyl cation intermediate in the electrocyclization sequence pathway.[4a−d,36] The second is from isomerization of a cation intermediate (Pt-containing 1,3,5-hexatriene) and then a direct or stepwise process to generate the product indene (Scheme 1). Although the metal−carbenoid and the metallacycle complexes in electrocyclization mechanisms have been previously proposed, we do not find "pure" examples among our stationary points along the mechanism, only **IM5** (Figure 2), which is a "mixed" metal−carbenoid and the metallacycle complex.[37] Yammamoto et al.[4a] reported a concerted insertion mechanism (Scheme 1) where 1-ethynyl-2-(1-alkoxybut-3-enyl)benzene is catalyzed by $PtBr_2$ to generate an indene. In our proposed mechanism, although the insertion sequence exists, it is a stepwise mechanism (**IM3** → **ts34** → **IM4** → **ts4Prod** → **Prod**). Additionally, it is shown in Figure 3 that the Pt−vinylidene **IM2** can be generated by another 4,5-hydrogen shift

dx.doi.org/10.1021/jo300849t | J. Org. Chem. 2012, 77, 6076−6086

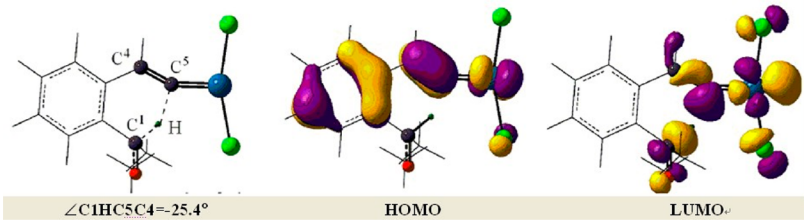

Figure 4. Selected Kohn−Sham orbital of **ts34**.

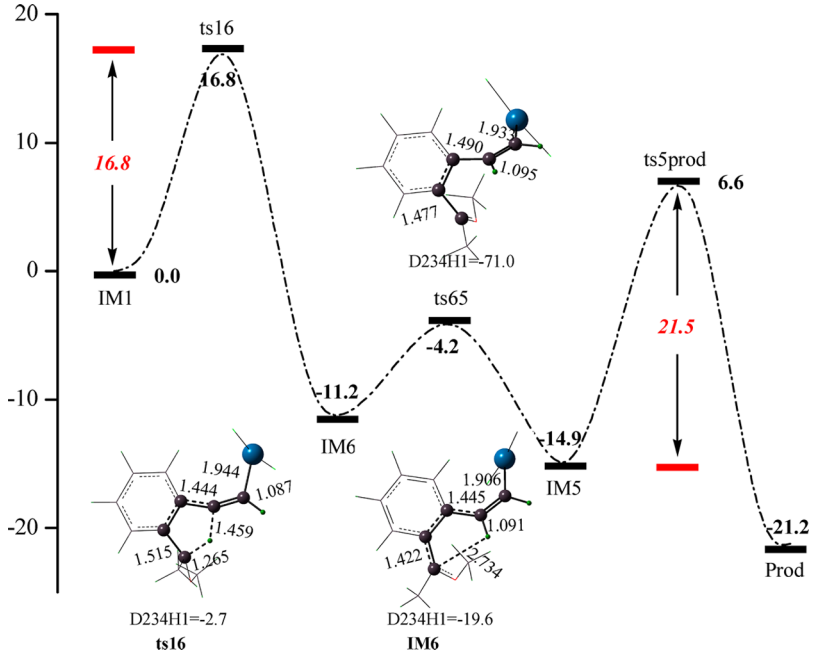

Figure 5. Energy profiles (kcal/mol) for Mechanism B. The relative free energies are given considering solvation effects [values were calculated at the B3LYP/PCM/6-31+G(d,p) (SDD for Pt)//B3LYP/6-31G(d) (6-31+G(d,p) for Cl; SDD for Pt) level using single-point PCM calculations to model the effect of the solvent (THF)]. (bond length, Å; angle, deg).

(**IM1** → **ts13**), but this pathway has a much higher activation free energy (about 34.5 kcal/mol) and is, therefore, infeasible.

In the C−H insertion mechanism of carbene, a concerted transition state requires that both p_x and p_y orbitals of carbene carbon atoms have strong interactions with the inserted C−H σ/σ^* orbitals. However, in Figure 4, the HOMO of **ts34** indicates that one of the most important contributions comes from the C5 p_y orbital. It should be noted that a near-zero MO coefficient of C1−H1 σ/σ^* character in the HOMO is found, meaning that the C5 p_y orbital has no bonding interaction with C1−H1 σ/σ^* orbitals. In contrast, one of the most important contributions in the LUMO comes from the C5 p_x atomic orbital. Another main contribution is derived from strong interactions of the C1−H1 σ/σ^* MOs with the C5 p_x orbital. Structurally, the C1, H1, C5, and C4 atoms are nearly in the same plane (−25.4°), and the C5 p_y orbital is nearly orthogonal to this plane, Therefore, only the hydride transfer occurs, and C1−C5 bond formation is not evident from **ts34**, which implies that the C−C bond formation was achieved through a stepwise pathway. A C1−C5 bond scan energy profile also verifies this; see the Supporting Information (page S29, Figure 2S). Overall, as shown in Figures 2 and 3, in the investigating system, the indene generated through the stepwise insertion mechanism of Mechanism A is feasible, and the formation of the Pt−vinylidene complex is the apparent rate-limiting step.[4a]

Additionally, it is reasonable to regard the region around 1,5-hydrogen shifting as the "critical geometry region", as well as to define the **IM3** as the "critical intermediate". The F reaction and the S reaction are bounded by the "critical intermediate" **IM3** (Figure 3). This diagram is also illustrated by the discussion in section 3.4.

3.2. Mechanism B: 1,4-Hydrogen Shift Mechanism. Despite experimental work where the through-space 1,5-hydrogen transfer is proposed to be a viable mechanism for the $PtCl_2$-catalyzed cyclization of aryl alkynes,[4a−c] He et al. point out that the 1,4-hydrogen migration pathway is also a possibility.[4d] Therefore, we have further explored the 1,4-hydrogen shift process. Figure 5 illustrates the selected optimized structures and the energy profile. It can be seen that Mechanism B has the same preliminary intermediate (**IM1**) as Mechanism A. The directed 1,4-hydrogen shifting process is somewhat disfavored because the free energy barrier of **ts16** is 16.8 kcal/mol, which is 3.4 kcal/mol higher than that of the 4,5-hydrogen shift in Mechanism A. While the 1,4-hydrogen migrates completely in **IM6**, the bond C4−H1 forms, which is verified by its bond length of 1.091 Å. From Figure 5, **IM6** is 28.0 kcal/mol lower in energy than **ts16** and 11.2 kcal/mol lower than that of **IM1**. Comparing the relative energies of **IM2** and **IM6** in Figures 3 and 5, respectively, although the energy of **IM6** is lower than that of **IM2** by 13.8 kcal/mol, it is only 1.8 kcal/mol higher than **IM4**. The intermediate **IM6** has similar characteristics to **IM4**. That is,

dx.doi.org/10.1021/jo300849t | J. Org. Chem. 2012, 77, 6076−6086

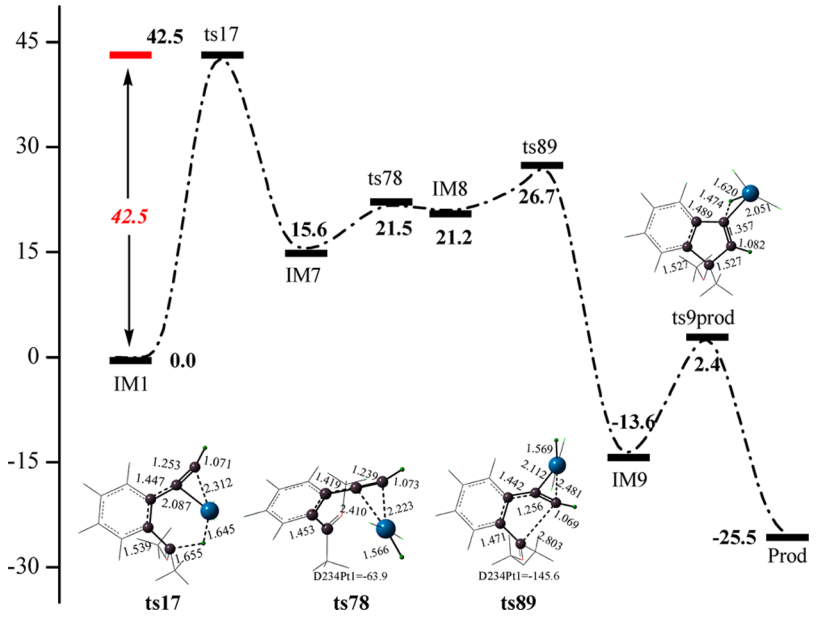

Figure 6. Energy profiles (kcal/mol) for Mechanism C. The relative free energies are given considering solvation effects [values were calculated at the B3LYP/PCM/6-31+G(d,p) (SDD for Pt)//B3LYP/6-31G(d) (6-31+G(d,p) for Cl; SDD for Pt) level using single-point PCM calculations to model the effect of the solvent (THF)]. (bond length, Å; angle, deg).

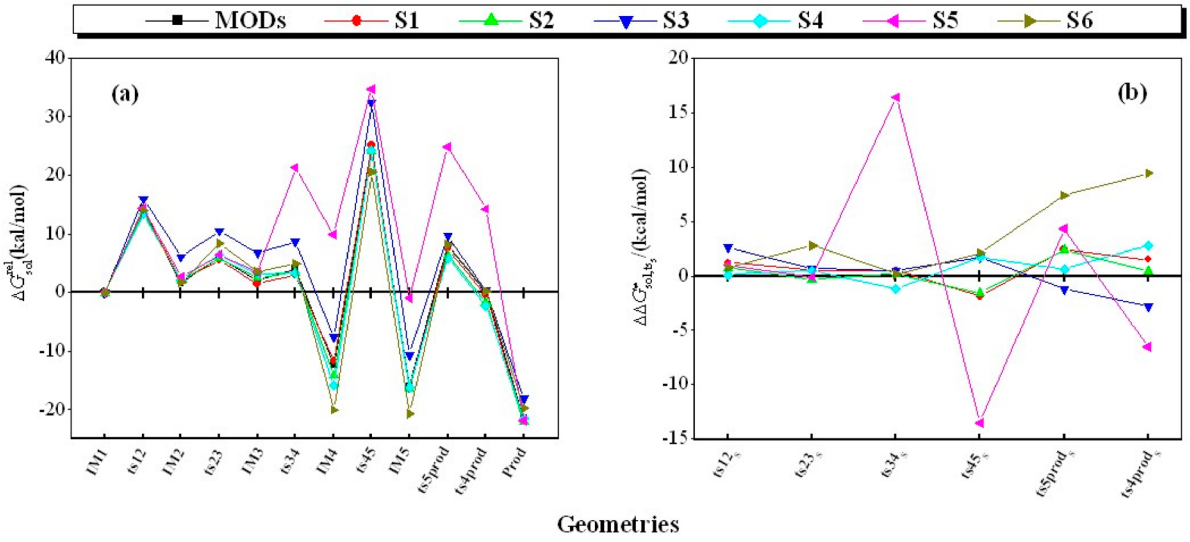

Figure 7. Effect of the substitution on Mechanism A. The energies are given in kcal/mol considering solvation effects.

both of them are benzyl cation intermediates and the natural charges of C1 in them are nearly equivalent (0.595 and 0.592 e, respectively, in **IM6** and **IM4**). Further, with a 7.0 kcal/mol energy barrier, **IM6** goes through **ts65**, and **IM5** is generated, accompanied by dihedral angle D234H1 rotation. The reaction path of Mechanism B merges with Mechanism A at this point. Overall, both of **IM1** → **ts16** → **IM6** and **IM5** → **ts5Prod** → **Prod** have a higher barrier than those of Mechanism A (by at least 3.4 kcal/mol). Therefore, Mechanism B may be ruled out, which agrees with mechanistic proposals from the literature.[4a−c]

3.3. Mechanism C: Catalyst-Aided 1,4-Hydrogen Shift Mechanism. Another mechanistic possibility arises because platinum-catalyzed cyclization of alkynes commonly occurs with accompanying migration of hydrogen or other groups.[4d,7] Yammamoto et al.[11] point out that the catalytic cyclization of *o*-alkynylbenzaldehyde acetals to functionalized indenes can occur via catalyst-aided methoxy transfer. Also, He and co-authors[4d] show that the intramolecular cyclization of *o*-substituted aryl alkynes through C(sp^3)−H activation can be completed via a catalyst-aided 1,4-hydrogen shift process. Inspired by these ideas, a potential mechanistic scenario (catalyst-aided 1,4-hydrogen shift mechanism: Mechanism C) is considered.

The selected optimized geometries and the energy profile for this process are represented in Figure 6 (for the other geometries, see the Supporting Information, page S2). In He's model,[4d] a reasonable first step of Pt-aided hydrogen transfer is $PtCl_2$ electrophilic attack of the C(sp^3)−H bond. Next, is subsequent addition of the alkyl−Pt to the alkyne and protonation, which affords the product indene. Our computations suggest that Mechanism C also involves the preliminary intermediate **IM1**. From **IM1** to **ts17**, the structural changes are quite different compared with Mechanism A and Mechanism B. For example, the dihedral angle D234Pt1 changes from +96.7° to −2.9°. The

dx.doi.org/10.1021/jo300849t | J. Org. Chem. 2012, 77, 6076−6086

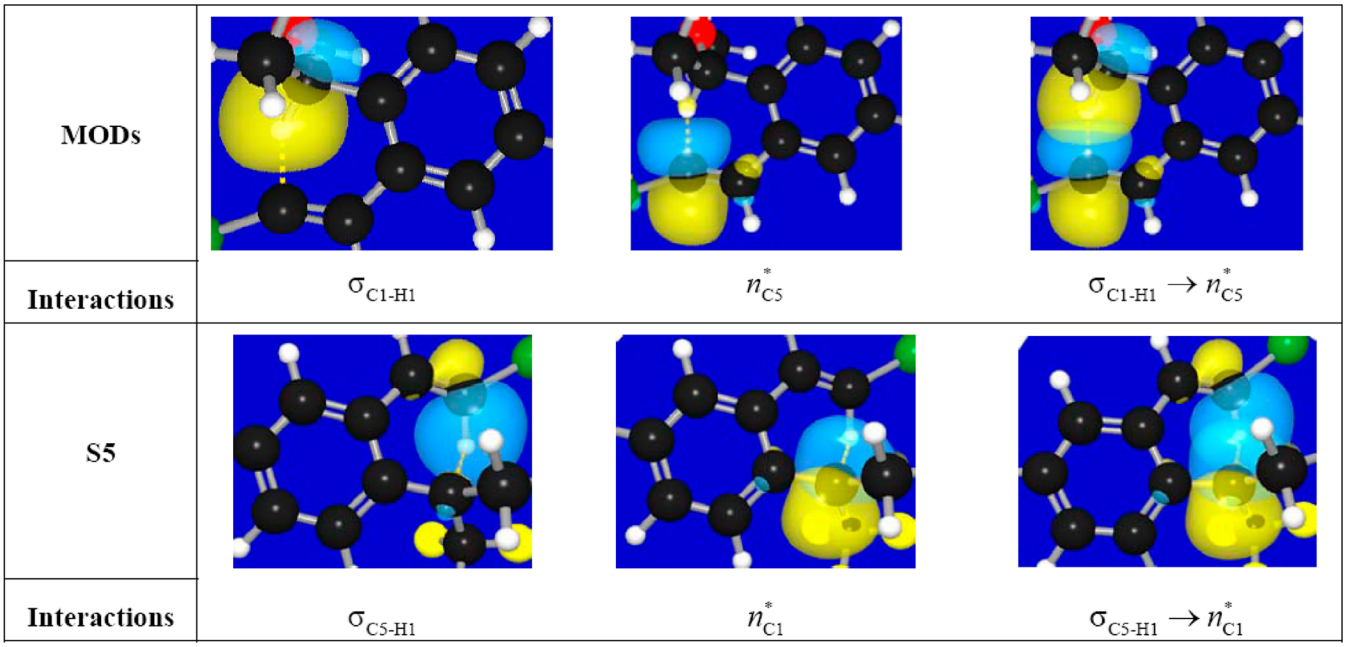

Figure 8. Three-dimensional (3D) plot of the NBOs of electron transfers for the two complexes of **ts34** and $\mathbf{ts34}_{S5}$ (**S5**).

structure **ts17** also possesses two active rings, a three-membered and a six-membered ring, with the original benzene ring in the same plane. From **IM1** to **ts17**, the H1 abstraction occurs over a long distance. Also, because of steric hindrance,[38] **ts17** has a much higher activation free energy of 42.5 kcal/mol. The dihedral angle D234Pt1 changes further along the mechanistic pathway, from −16.2° in **IM7** to −63.9° in **ts78**, to −85.8° in **IM8**, to −145.6° in **ts89**, and finally to −177.0° in **IM9**, when the dihedral rotation is completed.[39] In **IM9**, the interactions of $\sigma_{C4-Pt} \rightarrow \sigma^*_{H1-Pt}$ and $\sigma_{H1-Pt} \rightarrow \sigma^*_{H1-Pt}$ are strengthened ($E^{(2)}_{ij}$ = 58.8 and 34.8 kcal/mol, respectively), while the electron occupancy of σ_{C4-Pt} and σ_{H1-Pt} is reduced. Similarly, the occupancy of the σ^*_{H1-Pt} MO increases in **ts9Prod**,[40] which results in the H1−Pt and C4−Pt bond-breaking. This further spurs the H1 shift from Pt to C4, and **ts9Prod** has a free energy of activation of 16.0 kcal/mol. Overall, this pathway cannot be implicated in the mechanism because of its higher initial free energy of activation (about 43 kcal/mol).

3.4. Effect of the Substitution. In the original experiment,[4b,d,7b] the authors employed different substituents, such as CF_3 and OMe, on the substrate to investigate the substituent group effect upon the reaction mechanism. To qualitatively examine the substituent effect, the insertion reaction pathways of Mechanism A for the electron-rich group OMe− and electron-withdrawing group CF_3-substituted MODs (**S1**−**S6**, Scheme 2) were calculated. Figure 7a,b shows the relative free energy ΔG^{rel}_{sol} and the relative free energy barriers $\Delta\Delta G^{\ddagger}_{sol,ts_S}$ of Mechanism A, respectively.[41]

First, we focus on the substituent effect at benzene ring positions X and Y (Scheme 2). The activation free energies of Mechanism A are mostly insensitive to the substituent groups at the X and Y positions, except at the final step of the mechanism ($\mathbf{IM4}_S \rightarrow \mathbf{ts4Prod}_S \rightarrow \mathbf{Prod}_S$). With CF_3 substitution at the X position (**S1**), the activation free energy of $\mathbf{ts4Prod}_{S1}$ is increased by 1.5 kcal/mol and the initial activation energy of $\mathbf{ts12}_{S1}$ is also raised by 1.2 kcal/mol. In contrast, with OMe substitution at the X position (**S3**), the activation free energy of the final step of the mechanism is decreased by 2.9 kcal/mol, while the activation energies of $\mathbf{ts12}_{S3}$ and $\mathbf{ts23}_{S3}$ are increased by 2.6 and 0.7 kcal/mol, respectively. These examples indicate that substitution by electron-donating/electron-withdrawing groups at the X position has a slighter effect on the thermodynamic properties of the F reaction of Mechanism A. In contrast, when introducing electron-donating substituents on the Y position (OMe, **S4**), the activation energy of $\mathbf{ts4Prod}_{S4}$ is increased by 2.7 kcal/mol.

Second, the substituent effect at the benzyl sp^3 C atom is considered. When the Z position bears a CF_3 substituent (**S5**), after undergoing $\mathbf{IM3}_{S5}$, the thermodynamic properties of the mechanism can change dramatically. The activation free energy of $\mathbf{IM3}_{S5} \rightarrow \mathbf{IM4}_{S5}$ (17.8 kcal/mol) is much higher than that of the original case (1.4 kcal/mol), while the $\mathbf{ts4Prod}_{S5}$ activation energy is decreased by 6.5 kcal/mol. The $\mathbf{IM4}_{S5} \rightarrow \mathbf{ts4Prod}_{S5} \rightarrow \mathbf{Prod}_{S5}$ activation free energy is 4.4 kcal/mol. In **IM3** and $\mathbf{IM3}_{S5}$, the electron transferring from σ_{C1-H1} to n^*_{C5} can decrease the C1−H1 bond strength as well as assist the 1,5-hydrogen shifting. This transfer can be attributed to the $E^{(2)}_{ij}$ of **IM3** that is 1 kcal/mol larger than that of $\mathbf{IM3}_{S5}$. The NPA charges of C5, C1, and H1 atoms are 0.193, 0.174, and −0.361 e ($\mathbf{IM3}_{S5}$) and 0.097, 0.269, and 0.215 e (**IM3**). This suggests difficulty in transferring the H1 from C1 to C5 in $\mathbf{IM3}_{S5}$. Also, because the C1−H1 bond is strengthened, and the distance between H1 and C5 is increased in $\mathbf{IM3}_{S5}$,[42] the H1 transfer from C1 to C5 is quite difficult. This explains the very high free energy of activation in $\mathbf{ts34}_{S5}$.

When Z = CF_3, the C5−H1 bond length in the 1,5-hydrogen shift transition state $\mathbf{ts34}_{S5}$ is 1.220 Å (C1−H1 length: 1.517 Å) compared with **ts34** [1.575 Å (C1−H1 length: 1.183 Å)]. The interaction energy of $\sigma_{C5-H1} \rightarrow n^*_{C1}$ ($E^{(2)}_{ij}$ = 75.3 kcal/mol) in $\mathbf{ts34}_{S5}$ is significantly higher than $\sigma_{C1-H1} \rightarrow n^*_{C5}$ ($E^{(2)}_{ij}$ = 2.7 kcal/mol) of **ts34** (Figure 8). These structural and orbital features reveal that the transition structures **ts34** take on more reactant-like character, while $\mathbf{ts34}_{S5}$ possesses product-like character. This validates that $\mathbf{ts34}_{S5}$ should have a higher activation free energy than **ts34** due to the Hammond postulate.[43] As for **IM4** and $\mathbf{IM4}_{S5}$, the OMe substituent can stabilize the benzyl cation intermediate **IM4**. The relative energy of **IM4** (−13.0 kcal/mol) is 22.9 kcal/mol lower than that of $\mathbf{IM4}_{S5}$ (9.9 kcal/mol),

dx.doi.org/10.1021/jo300849t | J. Org. Chem. 2012, 77, 6076−6086

indicating that the **IM4**$_{S5}$ has stronger cyclization capability. The energy barriers of **ts4Prod**$_{S5}$ (4.4 kcal/mol) and **ts45**$_{S5}$ (24.9 kcal/mol) are lower by 6.5 and 13.5 kcal/mol than that of **ts4Prod** and **ts45**, respectively, although the C1−C5 length of **IM4**$_{S5}$ is much longer[44] and the relative free energies of **ts4Prod**$_{S5}$ (14.3 kcal/mol) and **ts45**$_{S5}$ (34.8 kcal/mol) are still quite large.

From the electronic structure of the subsequent transition state **ts5Prod**$_{S5}$, the $\Delta\Delta G^{\ddagger}_{sol,ts5Prod_{S5}}$ is positive (4 kcal/mol). This may also be due to the Hammond postulate[43] because the structure of **ts5Prod**$_{S5}$ is more product-like than that of **ts5Prod**, with the C1−C5 bond length of 2.310 and 2.119 Å, respectively. Moreover, in the energy profile **S5**, it is interesting that the rate-limiting step is changed from the 4,5-hydrogen shift to the 1,5-hydrogen shift, because the activation energy of **ts34**$_{S5}$ (17.8 kcal/mol) is 3.4 kcal/mol higher than that of **ts12**$_{S5}$. Also, the relative free energy of **ts34**$_{S5}$ (21.3 kcal/mol) is about 7 kcal/mol higher than that of **ts12**$_{S5}$ (14.4 kcal/mol).

As for the **S6** (E = OMe) substituted case, **IM4**$_{S6}$ has a relatively low free energy compared with the unsubstituted case **IM4** (−20.0 vs −13.0 kcal/mol), since the introduction of electron-donating groups can stabilize the benzylic cation. We note that **IM4**$_{S6}$ and **IM5**$_{S6}$ have longer C1−C5 bond distances than **IM4** and **IM5** (2.873 vs 2.838 Å and 3.254 vs 3.014 Å), which leads to a weaker orbital interaction in σ(C5−H1) → n*(C1) and σ(C5−H1) → σ*(C1−Pt1). Therefore, the substituent energy barriers of both electrocyclization/elimination and insertion steps transition states **ts5Prod**$_{S6}$ and **ts4Prod**$_{S6}$ are higher by 7.4 and 9.4 kcal/mol than those in the unsubstituted situation. Overall, the presence of an electron-donating/electron-withdrawing group at the phenyl X, Y and at the sp^3 benzyl carbon (C1) Z, E positions of the substrates is expected to change the thermodynamic properties of the reaction, especially the S reaction of Mechanism A. When substituting electron-withdrawing (**S5**, Z = CF_3) or electron-donating (**S6**, E = OMe) groups at the benzyl carbon, the process of **IM5**$_{S5,S6}$ → **Prod**$_{S5,S6}$ has a higher free energy of activation by more than 4 kcal/mol. Therefore, these substituents disfavor the electrocyclization/elimination process.

4. CONCLUSION

Three suggested types of mechanisms, one that leads to the formation of a Pt(II) vinyl carbenoid (Mechanism A), one with a transition-state structure of directed 1,4-hydrogen shift (Mechanism B), and one with Pt-aided 1,4-hydrogen migration (Mechanism C), were investigated by using density functional theory. Our results indicate the following:

(1) The Pt(II) vinyl carbenoid insertion mechanism is stepwise (corresponding to the stepwise insertion mechanism of Mechanism A), which is more favorable for the cyclization of indenes than the other suggested mechanisms, such as the electrocyclization mechanism of Mechanism A, direct 1,4-hydrogen shift Mechanism B, and catalyst-aided 1,4-hydrogen shift Mechanism C.

(2) In the F reaction, the first step is 4,5-hydrogen transfer (**ts12**), which forms the Pt(II) vinyl carbenoid (**IM2**). **IM2** then isomerizes to another Pt(II) vinyl carbenoid (**IM3**) through **ts23**. In the S reaction, the Fischer-type carbene **IM3** involves a 1,5-hydrogen migration (**ts34**), leading to a benzyl cation intermediate (**IM4**). Lastly, the insertion is completed through a concerted step **IM4** → **ts4Prod** → **Prod**.

(3) Electron-withdrawing/electron-donating groups substituted at phenyl and benzylic C(sp^3) can change the thermodynamic properties of the S reaction, but the effects on relative free energies are small for the F reaction. Strong electron-withdrawing/electron-donating substituent groups, such as CF_3/OMe at benzylic C(sp^3), can potentially adjust the overall rate-limiting step. For example, the rate-limiting step in **S5** is the 1,5-hydrogen shift, but that in MODs is the 4,5-hydrogen shift.

(4) The interaction between Pt and MODs in precursor **IM1** may be an example of the DCD model.[45] NBO and AIM analyses reveal that the interaction nature between the Pt catalyst and MOD fragments is electrostatic in **IM1**, as well as specific orbital interactions that play a role in key intermediates, such as the initial complex **IM1** (σ_{C5-H2} interaction with σ^*_{C4-C5} and σ^*_{C3-C4}, and the $n^{(3)}_{pt} \overset{\pi_{\parallel}}{\rightarrow} \pi^*_{C4-C5}$) and benzyl cation intermediate **IM3** ($\sigma_{C1-H1} \rightarrow n^*_{C5}$).

■ ASSOCIATED CONTENT

Supporting Information

The complete citation for ref 14, the Cartesian coordinates for the calculated stationary structures, and the free energies for the transition and ground states obtained from the DFT calculations are given. This material is available free of charge via the Internet at http://pubs.acs.org.

■ AUTHOR INFORMATION

Corresponding Author

*E-mail: ceszhcy@mail.sysu.edu.cn.

Notes

The authors declare no competing financial interest.

■ ACKNOWLEDGMENTS

C.Z. gratefully acknowledges the National Natural Science Foundation of China (Grant Nos. 20973204, 21173273, J1103305) and the Guangdong Provincial Natural Science Foundation (No. 9351027501000003). N.J.D. acknowledges the Scholarship for International Young Scientists of the National Natural Science Foundation of China (Grant No. 20950110326). Z.-.FL. would like to thank colleagues at the Gansu Computing Center.

■ REFERENCES

(1) (a) Guo, Y.; Zhao, X. M.; Zhang, D. Z.; Murahashi, S. I. *Angew. Chem., Int. Ed.* **2009**, *48*, 2047. (b) Jia, Y. X.; Kundig, E. P. *Angew. Chem., Int. Ed.* **2009**, *48*, 1636. (c) Nebra, N.; Lisena, J.; Saffon, N.; Maron, L.; Martin-Vaca, B.; Bourissou, D. *Dalton Trans.* **2011**, *40*, 8912. (d) Fantasia, S.; Pasini, A.; Nolan, S. P. *Dalton Trans.* **2009**, 8107. (e) Ritleng, V.; Sirlin, C.; Pfeffer, M. *Chem. Rev.* **2002**, *102*, 1731. (f) Conejero, S.; Paneque, M.; Poveda, M. L.; Santos, L. L.; Carmona, E. *Acc. Chem. Res.* **2010**, *43*, 572. (g) Kakiuchi, F.; Kan, S.; Igi, K.; Chatani, N.; Murai, S. *J. Am. Chem. Soc.* **2003**, *125*, 1698.

(2) (a) Periana, R. A.; Taube, D. J.; Gamble, S.; Taube, H.; Satoh, T.; Fujii, H. *Science* **1998**, *280*, 560. (b) Chen, M. S.; White, M. C. *Science* **2007**, *318*, 783.

(3) (a) Doyle, M. P.; Duffy, R.; Ratnikov, M.; Zhou, L. *Chem. Rev.* **2010**, *110*, 704. (b) Hansen, J. H.; Gregg, T. M.; Ovalles, S. R.; Lian, Y.; Autschbach, J.; Davies, H. M. L. *J. Am. Chem. Soc.* **2011**, *133*, 5076.

(4) (a) Bajracharya, G. B.; Pahadi, N. K.; Gridnev, I. D.; Yamamoto, Y. *J. Org. Chem.* **2006**, *71*, 6204. (b) Odedra, A.; Datta, S.; Liu, R.-S. *J. Org. Chem.* **2007**, *72*, 3289. (c) Tobisu, M.; Nakai, H.; Chatani, N. *J. Org. Chem.* **2009**, *74*, 5471. (d) Yang, S.; Li, Z.; Jian, X.; He, C. *Angew. Chem.,*

Int. Ed. **2009**, *48*, 3999. (e) Lee, J. M.; Chang, S. *Tetrahedron Lett.* **2006**, *47*, 1375. (f) Kao, L. C.; Sen, A. *J. Chem. Soc., Chem. Commun.* **1991**, 1242. (g) Dangel, B. D.; Johnson, J. A.; Sames, D. *J. Am. Chem. Soc.* **2001**, *123*, 8149.

(5) Goldshleger, N. F.; Eskova, V. V.; Shilov, A. E.; Shteinman, A. A. *Zh. Fiz. Khim.* **1972**, *46*, 1353.

(6) (a) Chianese, A. R.; Lee, S. J.; Gagne, M. R. *Angew. Chem., Int. Ed.* **2007**, *46*, 4042. (b) Jensen, M. P.; Wick, D. D.; Reinartz, S.; White, P. S.; Templeton, J. L.; Goldberg, K. I. *J. Am. Chem. Soc.* **2003**, *125*, 8614. (c) Kloek, S. M.; Goldberg, K. I. *J. Am. Chem. Soc.* **2007**, *129*, 3460. (d) Ziatdinov, V. R.; Oxgaard, J.; Mironov, O. A.; Young, K. J. H.; Goddard, W. A., III; Periana, R. A. *J. Am. Chem. Soc.* **2006**, *128*, 7404.

(7) (a) Zou, Y.; Garayalde, D.; Wang, Q.; Nevado, C.; Goeke, A. *Angew. Chem., Int. Ed.* **2008**, *47*, 10110. (b) Nakamura, I.; Bajracharya, G. B.; Wu, H.; Oishi, K.; Mizushima, Y.; Gridnev, I. D.; Yamamoto, Y. *J. Am. Chem. Soc.* **2004**, *126*, 15423. (c) An, S. E.; Jeong, J.; Baskar, B.; Lee, J.; Seo, J.; Rhee, Y. H. *Chem.—Eur. J.* **2009**, *15*, 11837. (d) Nakamura, I.; Bajracharya, G. B.; Mizushima, Y.; Yamamoto, Y. *Angew. Chem., Int. Ed.* **2002**, *41*, 4328. (e) Wang, S.; Zhang, L. *J. Am. Chem. Soc.* **2006**, *128*, 14274. (f) Dubé, P.; Toste, F. D. *J. Am. Chem. Soc.* **2006**, *128*, 12062.

(8) (a) Oh, H. L.; Lee, C.-H. *Bioorg. Med. Chem. Lett.* **2011**, *21*, 1347. (b) Chanda, D.; Saikia, D.; Kumar, J. K.; Thakur, J. P.; Agarwal, J.; Chanotiya, C. S.; Shanker, K.; Negi, A. S. *Bioorg. Med. Chem. Lett.* **2011**, *21*, 3966. (c) Zargarian, D. *Coord. Chem. Rev.* **2002**, *233*, 157. (d) Leino, R.; Lehmus, P.; Lehtonen, A. *Eur. J. Inorg. Chem.* **2004**, 3201. (e) Akbulut, U.; Khurshid, A.; Hacioglu, B.; Toppare, L. *Polymer* **1990**, *31*, 1343.

(9) Barluenga, J.; Fañanás-Mastral, M.; Aznar, F.; Valdés, C. *Angew. Chem., Int. Ed.* **2008**, *47*, 6594.

(10) References 4a and 4c provide two rate-limiting stages for Pt(II)-catalyzed transformation of aryl alkyne derivatives into functionalized indenes through C(sp^3)−H activation. Bajracharya et al. pointed out that the formation of the Pt−vinylidene complex is the rate-limiting step, while the Tobisu group assumes the 1,5-hydrogen shift as the turnover-limiting step of catalytic cycloisomerization.

(11) Nakamura, I.; Mizushima, Y.; Gridnev, I. D.; Yamamoto, Y. *J. Am. Chem. Soc.* **2005**, *127*, 9844.

(12) As a model, it is suitable to study whether the OMe and the carbon−carbon triple bond can both coordinate with Pt in the initial intermediate. Also, it has been studied experimentally by Tobisu et al. (ref 4c).

(13) Parr, R. G.; Yang, W. *Density-Functional Theory of Atoms and Molecules*; Oxford University Press: Oxford, U.K., 1989.

(14) Frisch, M. J.; et al. *Gaussian 09*, revision A.01; Gaussian, Inc.: Wallingford, CT, 2009.

(15) (a) Becke, A. D. *Phys. Rev. A* **1988**, *38*, 3098. (b) Lee, C.; Yang, W.; Parr, R. G. *Phys. Rev. B* **1988**, *37*, 785. (c) Becke, A. D. *J. Chem. Phys.* **1993**, *98*, 5648.

(16) Becke, A. D. *J. Chem. Phys.* **1993**, *98*, 1372.

(17) (a) Jiao, L.; Lin, M.; Yu, Z.-X. *J. Am. Chem. Soc.* **2010**, *133*, 447. (b) Ando, K. *J. Org. Chem.* **2010**, *75*, 8516. (c) Xia, Y.; Huang, G. *J. Org. Chem.* **2010**, *75*, 7842. (d) Fang, R.; Su, C.-Y.; Zhao, C.; Phillips, D. L. *Organometallics* **2009**, *28*, 741.

(18) (a) Faza, O. N.; López, C. S.; Álvarez, R.; de Lera, A. R. *J. Am. Chem. Soc.* **2006**, *128*, 2434. (b) Shi, F.-Q.; Li, X.; Xia, Y.; Zhang, L.; Yu, Z.-X. *J. Am. Chem. Soc.* **2007**, *129*, 15503. (c) Yu, Z.-X.; Wender, P. A.; Houk, K. N. *J. Am. Chem. Soc.* **2004**, *126*, 9154.

(19) (a) Fukui, K. *Acc. Chem. Res.* **1981**, *14*, 363. (b) Fukui, K. *J. Phys. Chem.* **1970**, *74*, 4161.

(20) (a) Mineva, T.; Russo, N.; Sicilia, E. *J. Comput. Chem.* **1998**, *19*, 290. (b) Cossi, M.; Scalmani, G.; Rega, N.; Barone, V. *J. Chem. Phys.* **2002**, *117*, 43. (c) Tomasi, J.; Persico, M. *Chem. Rev.* **1994**, *94*, 2027.

(21) Glendening, E. D.; Badenhoop, J. K.; Reed, A. E.; Carpenter, J. E.; Bohmann, J. A.; Morales, C. M.; Weinhold, F. *NBO 5.0*; Theoretical Chemistry Institute, University of Wisconsin: Madison, WI, 2001.

(22) Keith, T. A. *AIMAll*, Version 11.06.09, 2011. http://aim.tgkristmill.com.

(23) Calculated levels a, b, c, and d denote B3LYP/6-31G(d) (6-31+G(d,p) for Cl; SDD for Pt), B3LYP/6-31+G(d,p) (SDD for Pt)//B3LYP/6-31G(d) (6-31+G(d,p) for Cl; SDD for Pt), B3LYP/6-31+G(d,p) (SDD for Pt)//B3LYP/6-31G(d,p) (6-31+G(d,p) for Cl; SDD for Pt), and BHandHLYP/6-31+G(d,p) (SDD for Pt)//BHandHLYP/6-31G(d) (6-31+G(d,p) for Cl; SDD for Pt), respectively.

(24) Vadola, P. A.; Sames, D. *J. Am. Chem. Soc.* **2009**, *131*, 16525.

(25) (a) Chatt, J.; Duncanson, L. A. *J. Chem. Soc.* **1953**, 2939. (b) Dewar, M. J. S. *Bull. Soc. Chim. Fr.* **1951**, *18*, C71. (c) Dedieu, A. *Chem. Rev.* **2000**, *100*, 543. (d) Nechaev, M. S.; Rayón, V. M.; Frenking, G. *J. Phys. Chem. A* **2004**, *108*, 3134. (e) Frenking, G.; Fröhlich, N. *Chem. Rev.* **2000**, *100*, 717. (f) Fürstner, A.; Davies, P. W. *Angew. Chem., Int. Ed.* **2007**, *46*, 3410.

(26) Bader, R. F. W. In *Atoms in Molecules: A Quantum Theory*; The International Series of Monographs of Chemistry; Halpern, J., Green, M. L. H., Eds.; Clarendon Press: Oxford, U. K., 1990.

(27) The motive power may be derived from the local steric repulsion between two occupied orbitals BD(C1−H1) and BD(C4−H2) with steric exchange energies d$E(i,j)$ = 3.88 kcal/mol.

(28) The main structural difference between **IM2** and **IM3** is the dihedral angle D234H2, being 13.4° and −177.0° respectively.

(29) It was performed by using the $DEL keylist of NBO.

(30) (a) Crabtree, R. H. *The Organometallic Chemistry of the Transition Metals*; Wiley: New York, 2005. (b) Occhipinti, G.; Jensen, V. R. *Organometallics* **2011**, *30*, 3522.

(31) Fischer, E. O.; Maasbol, A. *Angew. Chem., Int. Ed.* **1964**, *3*, 580.

(32) Schrock, R. R. *J. Am. Chem. Soc.* **1974**, *96*, 6796.

(33) The nature of the Fischer carbene bond is "ionic" (ref 30b). The Pt−C bond in **IM2** and **IM3** is dominated by the ionic contributioins (about 57% of the total natural bond order), which is obtained by using NRT analysis.

(34) Taylor, T. E.; Hall, M. B. *J. Am. Chem. Soc.* **1984**, *106*, 1576.

(35) (a) Nakamura, E.; Yoshikai, N.; Yamanaka, M. *J. Am. Chem. Soc.* **2002**, *124*, 7181. (b) Hansen, J.; Autschbach, J.; Davies, H. M. L. *J. Org. Chem.* **2009**, *74*, 6555.

(36) Jurberg, I. D.; Odabachian, Y.; Gagosz, F. *J. Am. Chem. Soc.* **2010**, *132*, 3543.

(37) It is also verified by the Pt−C1 bond scan energy profile.

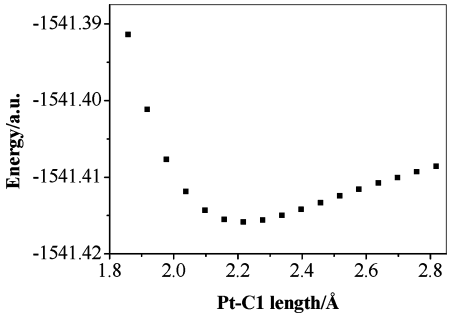

(38) The d$E(i,j)$ between BD(3)(C4−C5) and BD(1)(C1−H1) is 16.44 kcal/mol.

(39) The motive power may be derived from the local steric repulsion between BD(C1−H1) and n(2)(O), BD(C1−Pt1) and n(2)(O), BD(3)(C4−C5) and BD(H1−Pt1), and BD(C4−C5) and BD(H1−Pt1), with steric exchange energies d$E(i,j)$ = 11.24, 16.76, 18.78, 8.12, and 10.87 kcal/mol, respectively.

(40) The extent of change in the electron occupation of BD(C4−Pt) is decreased from 1.919 to 1.641, whereas that of BD*(H1−Pt) is increased from 0.132 to 0.449.

(41) The $\Delta\Delta G^{\ddagger}_{sol,ts_S}$ is defined as $\Delta\Delta G^{\ddagger}_{sol,ts_S} = \Delta G^{\ddagger}_{sol,ts_S} - \Delta G^{\ddagger}_{sol,ts}$. For example, the $\Delta\Delta G^{\ddagger}_{sol,ts12_{S1}} = \Delta G^{\ddagger}_{sol,ts12_{S1}} - \Delta G^{\ddagger}_{sol,ts12}$ = 14.5 − 13.4 = 1.1 kcal/mol.

(42) The bond length of C1−H1 is 1.107 and 1.095 Å in **IM3** and **IM3$_{SS}$**, respectively. The distance between H1 and C5 is 2.243 and 2.266 Å in **IM3** and **IM3$_{SS}$**, respectively. The bond strength is indexed by BO_N; it is greater by 0.002 in **IM3$_{SS}$** (0.9999) than that in **IM3** (0.9979). Therefore, the bond C1−H1 in **IM3$_{SS}$** is not easily broken. Because of

the long bond distance between H1 and C5, the H1 transfer from C1 to C5 is also very difficult compared with that in **IM3**.

(43) Hammond, G. S. *J. Am. Chem. Soc.* **1955**, *77*, 334.

(44) The C1−C5 length in $\mathbf{IM4}_{SS}$ and **IM4** is 3.049 and 2.838 Å, respectively.

(45) (a) Tiana, D.; Francisco, E.; Blanco, M. A.; Macchi, P.; Sironi, A.; Martín Pendás, A. *J. Chem. Theory Comput.* **2010**, *6*, 1064. (b) Linares, M.; Braida, B.; Humbel, S. *Inorg. Chem.* **2007**, *46*, 11390. (c) Barnett, N. J.; Slipchenko, L. V.; Gordon, M. S. *J. Phys. Chem. A* **2009**, *113*, 7474. (d) Michalak, A.; Mitoraj, M.; Ziegler, T. *J. Phys. Chem. A* **2008**, *112*, 1933. (e) Liu, Z. *J. Phys. Chem. A* **2009**, *113*, 6410.